Enabling Boomless CubeSat Magnetic Field Measurements with the Quad-Mag Magnetometer and Underdetermined Blind Source Separation

Alex Paul Hoffmann[1], Mark B. Moldwin[1], Brady P. Strabel[1], Lauro V. Ojeda[2]

[1]Climate and Space Sciences and Engineering, University of Michigan, Ann Arbor, Michigan
[2]Mechanical Engineering, University of Michigan, Ann Arbor, Michigan

Key Points:

- The Quad-Mag CubeSat magnetometer combined with the UBSS noise cancellation technique enable high-fidelity magnetic field measurements without the need for a boom.
- Quad-Mag instrument equipped with four magneto-inductive magnetometers has a resolution two times better than that of any single sensor.
- UBSS algorithm can remove stray magnetic field noise without prior knowledge of the magnitude, orientation, or number of noise sources.

Corresponding author: Alex Paul Hoffmann, aphoff@umich.edu

Abstract

In situ magnetic field measurements are often difficult to obtain due to the presence of stray magnetic fields generated by spacecraft electrical subsystems. The conventional solution is to implement strict spacecraft magnetic cleanliness requirements and place magnetometers on a deployable boom. However, this method is not always feasible on low-cost platforms due to factors such as increased design complexity, increased cost, and volume limitations. To overcome this problem, we propose using the Quad-Mag CubeSat magnetometer with an improved Underdetermined Blind Source Separation (UBSS) noise removal algorithm. The Quad-Mag consists of four magnetometer sensors in a single CubeSat form-factor card that allows distributed measurements of stray magnetic fields from electrical subsystems. The UBSS algorithm can remove stray magnetic field noise without prior knowledge of the magnitude, orientation, or number of noise sources. UBSS is a two-stage algorithm that identifies signals through cluster analysis and separates them through compressive sensing. We use UBSS with single source point (SSP) detection to improve the identification of noise signals and iteratively weighted compressed sensing to separate noise signals from the ambient magnetic field. Using a mock CubeSat, we demonstrate in the lab that UBSS reduces four noise signals producing more than 100 nT of noise at each magnetometer to below the expected instrument resolution (near 5 nT). Additionally, we also show that the integrated Quad-Mag and UBSS system works well for 1U, 2U, 3U, and 6U CubeSats in simulation. Our results show that the Quad-Mag and UBSS noise cancellation package enables high-fidelity magnetic field measurements from a CubeSat without a boom.

Plain Language Summary

Measuring magnetic fields in their natural space environment, or "in situ," can be difficult because of interference from other artificial magnetic fields. These other magnetic fields, called "stray magnetic fields," are often created by the electrical subsystems on the spacecraft. The usual way to solve this problem is by making sure the spacecraft is very clean magnetically and by putting special sensors on a long arm that sticks out from the spacecraft. However, this solution can be difficult to use on small spacecraft, such as CubeSats, because it makes the spacecraft more expensive and harder to design. In this study, we propose an alternative solution by using a special sensor called Quad-Mag and a method to cancel out noise called Underdetermined Blind Source Separation (UBSS). This new solution allows accurate measurements without the need for a long arm and it works well even on CubeSats. The combination of Quad-Mag and UBSS technology has the potential to revolutionize CubeSat magnetometry, offering valuable opportunities for space research and exploration.

1 Introduction

In situ magnetic field measurements are essential for studying the dynamics of space plasmas in the near-Earth environment. These measurements allow us to observe various currents in the magnetosphere, such as field-aligned currents (FACs) and magnetopause currents. The Enhanced Plasma Outflow Probe, for example, detects FACs and enables research into how the magnetospheric and ionospheric systems are coupled (Wallis et al., 2015). However, obtaining accurate measurements of the ambient magnetic field in space can be challenging due to stray magnetic fields from spacecraft subsystems. Spacecraft subsystems, including solar panels, magnetorquers, batteries, and propulsion systems, generate stray magnetic fields that interfere with measurements of the ambient magnetic field (Finley et al., 2023). For Instance, the GOES-16 spacecraft employs electric propulsion-based thrusters that generate about 20 nT of stray magnetic field noise (Califf et al., 2020). These noise signals inhibit space physics research that utilizes magnetic field measurements.

The historical way to mitigate stray magnetic fields in magnetometer measurements is to use strict magnetic cleanliness requirements and a deployable boom that extends the magnetometer away from the spacecraft. For example, the Voyager spacecraft has a 13-meter-long boom that reduces noise from the spacecraft body to less than 0.2 nT (Miller, 1979). However, booms do not guarantee noise elimination, as shown by some difficulties encountered by the Defense Meteorological Satellite Program (DMSP), which uses a single magnetometer mounted on a 5-meter boom (Kilcommons et al., 2017). Moreover, booms introduce significant design complexity and cost that can make them unsuitable for CubeSat applications. As a result, some space exploration missions are not equipped with magnetometers.

The use of multiple magnetometers on a spacecraft enables the application of noise cancellation algorithms to separate stray magnetic fields from the ambient magnetic field. Several gradiometry algorithms have been developed which model the spacecraft noise as a magnetic dipole and use a pair of magnetometers to remove the estimated noise (Ness et al., 1971; Carter et al., 2016; Ream et al., 2021). However, these algorithms still require the use of a mechanical boom. As the use of CubeSats for space physics research are rising in popularity, a magnetometer package that fits the form factor and economic requirements of a CubeSat are necessary. We propose the use of the Quad-Mag magnetometer board and a noise cancellation technique called Underdetermined Blind Source Separation (UBSS) to remove stray magnetic field noise from CubeSat Magnetometer Measurements.

The Quad-Mag is a 10 cm x 10 cm board that is composed of four separate PNI RM3100 magnetometers (Strabel et al., 2022). The PNI RM3100 is a commercial magnetometer that samples the magnetic field using magneto-inductive sensing (Leuzinger & Taylor, 2010). The sensor is composed of an ASIC and a simple oscillator circuit, and can measure down to 2.7 nT at 1 Hz (Regoli et al., 2018). The use of four magnetometers allows for a reduction in the measurement uncertainty of the PNI RM3100 by a factor of 2. The Quad-Mag board has a total power consumption of only 23 mW when active and can measure magnetic fields within a resolution of near 1 nT at 1 Hz.

The presence of multiple magnetometers also enables the use of the UBSS algorithm to separate stray magnetic field noise generated by spacecraft subsystems. The UBSS algorithm models the presence of noise signals in the magnetometer measurements through the following system.

$$B(t,k) = KS(t,k) \tag{1}$$

In this system the source signals, $S(t,k)$, at the time-frequency bin, (t,k), mix into the magnetometer signals, $B(t,k)$. The presence of each source signal at each magnetometer is defined by the mixing matrix, K. The UBSS algorithm is a two-step algorithm that identifies the mixing matrix, K, through cluster analysis and separates the source signals from the mixed signals via compressive sensing. Hoffmann and Moldwin (2022) demonstrated the removal of four noise signals from lab-generated magnetometer data and reduced the root mean squared error (RMSE) of magnetometer measurements from 300.53 nT to 7.23 nT (near the sensor resolution at 50 Hz). The UBSS algorithm can remove stray magnetic field noise without prior knowledge of the magnitude, orientation, or number of noise sources. This novel approach allows us to obtain high-fidelity magnetic field measurements with a greater degree of accuracy and precision.

In this work, we present two experiments demonstrating the Quad-Mag and UBSS system. The first experiment demonstrates using a mock CubeSat, the separation of four copper coil-generated noise signals from SWARM magnetometer data. The second experiment simulates the removal of noise measured by the Quad-Mag in 1U, 2U, 3U, and 6U CubeSats. We also present several enhancements to the noise removal algorithm by Hoffmann and Moldwin (2022), detailed in the methodology section. The successful application of the Quad-Mag magnetometer with UBSS would enable high-fidelity mag-

netic field measurements to be recorded from a CubeSat without the need for a boom. This solution not only improves the accuracy of magnetic field measurements, but it also significantly reduces the cost and complexity of spacecraft designed to measure the magnetic fields of space plasma.

2 Methodology

The Quad-Mag is a low size, weight, power, and cost (SWAP-C) magnetometer that enables high-fidelity magnetic field measurements and fits the form factor of a CubeSat. The UBSS algorithm, designed by Hoffmann and Moldwin (2022), allows for the use of the Quad-Mag in the noisy CubeSat environment expected for a magnetometer mounted inside the CubeSat bus. In this section, we provide an overview of the specifications of the Quad-Mag designed by Strabel et al. (2022), and the UBSS algorithm designed by Hoffmann and Moldwin (2022). We also describe several improvements made to the UBSS algorithm through the implementation of Single Source Point Detection, changing the clustering algorithm, and introducing an iterative weighting scheme to the compressive sensing algorithm in signal reconstruction.

2.1 The Quad-Mag Techniques and Specifications

The Quad-Mag is a 10 cm x 10 cm standard CubeSat form factor board composed of four PNI RM3100 magnetometers. The Quad-Mag board weighs 59 grams and consumes 23 mW of power when active. For an individual axis, it has a noise floor of 3.770 pT $\sqrt{Hz}^{-1}$ at 1 Hz. It is important to note that various methods can be used to calculate the noise floor, leading to different outcomes. In this case, the noise floor was determined by Strabel et al. (2022) using the power spectral density derived from the frequency-transformed auto-correlation of the measured magnetometer signal. The PNI RM3100 magnetometers are synchronized and controlled by a single MSP430 microcontroller. The Quad-Mag also uses a simple UART interface to send telemetry and receive commands to and from the CubeSat.

The PNI RM3100 is a digital magnetometer that measures ambient magnetic field via a relaxation oscillator composed of a digitally emulated Schmitt trigger and resistor-inductor circuit, as seen in Figure 1.

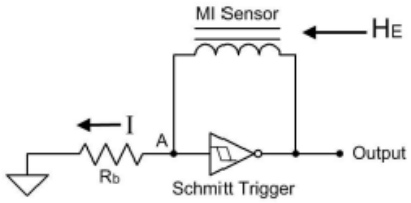

Figure 1: Schematic of the magneto-inductive sensing circuit by Leuzinger and Taylor (2010)

The PNI RM3100 uses an ASIC to emulate the behavior of the Schmitt trigger. This circuit measures the magnetic field through repeatedly driving the inductor into saturation in the forward and reverse directions. The presence of an ambient magnetic field biases the inductor in one direction and shortens the time necessary to drive the circuit into saturation in that direction. The forward and reverse cycles drive counter

circuits whose difference can be used to reconstruct the ambient magnetic field. This process is illustrated in Figure 2.

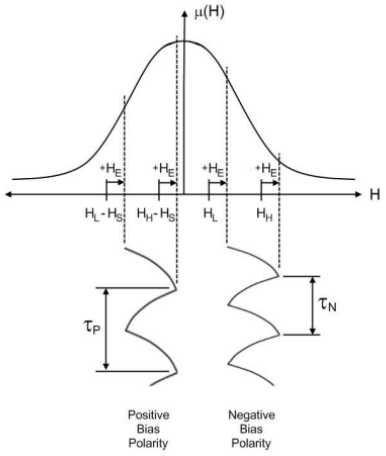

Figure 2: Illustration of the saturation time asymmetry due to an applied external field by Leuzinger and Taylor (2010)

The PNI RM3100 is a commercial magnetometer but has been proven to be spaceflight-ready. The PNI RM3100 was shown to be radiation tolerant when irradiated up to 150 kRad total ionizing dose, and resistant up to 76.7 MeV cm^2 mg^{-1} for single event latch-up (Regoli et al., 2020; Moldwin et al., 2022). As the magnetic field is sensed through digital counters, the measurement uncertainty of the magnetometer has a dependence on the sampling frequency. Regoli et al. (2018) characterized the PNI RM3100 and observed a measurement uncertainty of 8.7 nT at 40 Hz, 2.7 nT at 1 Hz, and a linear dynamic range of ±100,000 nT. During testing in the University of Michigan's Magnetic Laboratory, we tested several PNI RM3100 magnetometers and found the measurement uncertainty of individual sensors to be between 1.5 nT and 2.5 nT at 1 Hz. The variance is a result from the mass manufacturing process. To account for this, we have developed a procedure to find the best performing sensors from different production batches to use for flight missions.

The use of four PNI RM3100 magnetometers on the Quad-Mag board has multiple purposes. First, the Quad-Mag is able to achieve a lower measurement uncertainty than a single magnetometer through averaging. The measurement uncertainty decreases with respect to $\sqrt{M}$ where M is the number of magnetometers. Strabel et al. (2022) observed a measurement uncertainty of 5.34 nT when sampling the Quad-Mag at 65 Hz versus 10.59 nT when testing a single PNI RM3100. The second advantage of using four magnetometers is that multiple points of measurement enable the use of noise cancellation algorithms such as UBSS. This paper demonstrates that the short distance separation of the four magnetometers on the Quad-Mag is sufficient to identify multiple noise sources within a CubeSat.

2.2 Signal Preprocessing

The role of UBSS in magnetic noise removal is to separate out the spacecraft-generated noise from the ambient magnetic field if there are more noise sources than magnetometers (Hoffmann & Moldwin, 2022). UBSS is a blind algorithm which means that it does not require any prior knowledge of the magnitude, spectral content, location, or orien-

tation of the noise sources. However, in spacecraft magnetometry we assume that the ambient magnetic field appears equally at each magnetometer. At the time-frequency bin, (t, k), the presence of the source signals, $S(t, k)$, at each magnetometer, $B(t, k)$, is defined by the mixing system, $B(t, k) = KS(t, k)$, where K is the mixing matrix and its columns are known as the mixing vectors. This system is expressed in its full matrix format in equation (2).

$$\begin{bmatrix} B_1(t,k) \\ B_2(t,k) \\ \vdots \\ B_m(t,k) \end{bmatrix} = \begin{bmatrix} 1 & k_{12} & k_{13} & ... & k_{1n} \\ 1 & k_{22} & k_{23} & ... & k_{2n} \\ \vdots & \vdots & \vdots & \ddots & \vdots \\ 1 & k_{m2} & k_{m3} & ... & k_{mn} \end{bmatrix} \begin{bmatrix} S_1(t,k) \\ S_2(t,k) \\ \vdots \\ S_n(t,k) \end{bmatrix} \tag{2}$$

In this system, we seek to recover the ambient magnetic field signal, $S_1(t, k)$, which is associated with the column of ones in the mixing matrix, K. The system can be expressed as b=Ks, where K is a wide matrix and s is a vector of source signals. However, this system is underdetermined and has infinitely many solutions. For instance, if s is a solution to b=Ks, then so is s+s', where s' belongs to the null space of K. The UBSS algorithm uses a two-step approach to overcome this challenge. The first step identifies the source signals by finding their corresponding mixing vectors in K using cluster analysis. The second step separates the ambient magnetic field signal by applying compressive sensing techniques.

Both steps rely on the sparsity assumption that only one signal is active in a time-frequency bin (t,k). If $S_j(t, k)$ is the only active signal at time-frequency, (t, k), and all other signals are zero, then the system in equation 2 can be simplified to a single mixing vector.

$$\begin{bmatrix} B_1(t,k) \\ B_2(t,k) \\ \vdots \\ B_m(t,k) \end{bmatrix} = \begin{bmatrix} k_{1j} \\ k_{2j} \\ \vdots \\ k_{mj} \end{bmatrix} S_j(t,k) \tag{3}$$

The reduced system in equation 3 defines a straight line with a slope proportional to the mixing vector, K_j. If the mixed magnetometer signals, $B(t, k)$ are scatter plotted against each other, then each sparse source signal will form a line defined by their corresponding mixing vectors. An example of this can be seen below in Figure 3.

In order to discover the mixing vector corresponding to each noise signal, we define a space, $\mathbf{H} \in \mathbb{R}^{2m}$, where each magnetometer, m, and the relative phase of each magnetometer signal is a dimension. The relative phase is defined in section 2.3 and is used to find the polarity of the elements of the mixing matrix.

2.3 Noise Identification through Cluster Analysis

The magnetometer measurements, $b(t)$, must be filtered and transformed into a clusterable format in order to perform cluster analysis. Magnetometer data are rarely sparse in the time domain, so the Non-Stationary Gabor Transform (NSGT) of the magnetometer signals are taken in order to transform the signals into a sparse domain (Holighaus et al., 2013). This transform is similar to a Short Time Fourier Transform (STFT), but it improves the spectral resolution of the transform through evolving the window size with respect to frequency. This effect makes the NSGT transform similar to a wavelet transform.

Once the mixed magnetometer signals, $B(t, k)$, have been obtained, the mixed signals are projected to the surface of a unit hypersphere through equation 4.

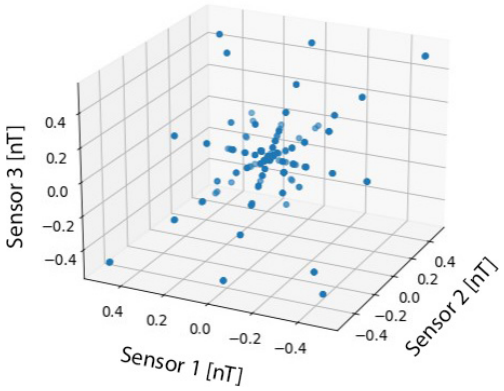

Figure 3: Three mixed signals composed of six sparse source signals scatter plotted against each other (Figure by Hoffmann and Moldwin (2022)).

$$B^*(t,k) := \frac{|B(t,k)|}{\|B(t,k)\|} \tag{4}$$

Through equation 4, the transformed time-frequency points will form densely packed clusters on the surface of a unit hypersphere. The centroid of these clusters is proportional to the mixing vectors of each source signal. Figure 4 shows the mixed signals from Figure 3 transformed through equation 4.

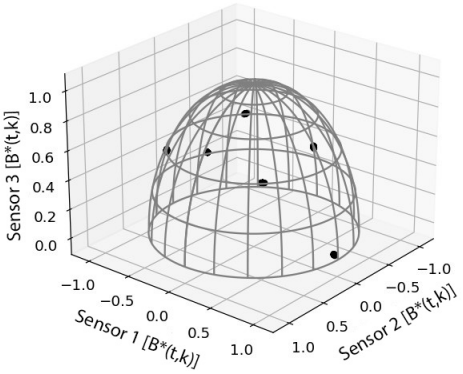

Figure 4: Time-frequency points from three mixed signals in Figure 1 projected onto a unit hyperspace. The compactly formed clusters are proportional to the mixing vectors of the corresponding noise signals (Figure by Hoffmann and Moldwin (2022)).

The projected time-frequency points form clusters that are used to reconstruct the columns of the mixing matrix, K. However, the measurement uncertainty and presence of multi-source points (MSP) may cause the signals, $B(t,k)$, to project randomly and obscure the relevant clusters. Two filters are applied to the magnetometer data before cluster analysis is performed in order to overcome these constraints.

The measurement uncertainty of the PNI RM3100 magnetometer at 1 Hz is near 2.7 nT. As a result, time-frequency bins with low energy may project randomly onto the unit hypersphere (Sun et al., 2016). We cleanse these low energy data points using a magnitude filter which removes data points below a factor of the magnetometers measurement uncertainty. This filter is defined in equation 5.

$$|B(t,k)| > \lambda \cdot \sigma \tag{5}$$

The parameter, σ, defines the standard deviation of the characterized measurement uncertainty of the magnetometer. The variable, λ, is the factor that defines the magnitude at which low energy points should be removed with respect to the measurement uncertainty, σ. Only statistically meaningful data points will remain after the magnitude filter has been applied.

To identify and remove multi-source points (MSPs), we use a single source point (SSP) detection algorithm that compares the complex and real components of the mixed magnetometer signals, $B(t,k)$. If only one source signal, $S_j(t,k)$, contributes to a time-frequency bin, (t,k), then both the real and imaginary components of $B(t,k)$ will be proportional to the same mixing vector, K_j. This means that their cosine similarity will be equal to 1. We calculate the cosine similarity using equation 6 and remove data points that are above a certain threshold, θ_0 (Reju et al., 2009).

$$\theta = cos^{-1}\left(\frac{\{Re[B(t,k)]\}^T Im[B(t,k)]}{\sqrt{\{Re[B(t,k)]\}^T Re(B(t,k))}\sqrt{\{Im[B(t,k)]\}^T Im(B(t,k))}}\right) \tag{6}$$

After the low energy and multi-source points are removed from $B^*(t,k)$, the last step in processing the data into a clusterable format is to join the signals, $B^*(t,k)$ with their relative phase in order to find the source signal polarities. The transform in equation 4 strips the data points of their polarity, so take the relative phase defined in equation 7 in order to reconstruct the polarity of the mixing vector components.

$$\arg B(t,k) = \{\arg B_j(t,k) - \arg\left(B_0(t,k) \mid j \in [0,m]\right\} \tag{7}$$

Using the result of equation 7, a new data format, H(t,k), is defined by concatenating the projected magnitude data with the argument of the time-frequency data.

$$H(t,k) = (B^*(t,k), \arg\left(B(t,k)\right)) \tag{8}$$

Once the original magnetometer data, $b(t)$, has been transformed into a clusterable format, $H(t,k)$, an array of clustering algorithms can be used to reconstruct the mixing matrix, K. Hoffmann and Moldwin (2022) use the Density Based Spatial Clustering for Applications with Noise (DBSCAN) algorithm (Ester et al., n.d.). This algorithm requires two data-dependent parameters, *eps* and *minPts*, that must be set by the user. In this work, we use the Hierarchical Density Based Spatial Clustering for Applications with Noise (HDBSCAN) algorithm because it has similar benefits to DBSCAN but does not require the user to set any parameters (McInnes & Healy, 2017; Campello et al., 2013). HDBSCAN is an extension of DBSCAN that uses a hierarchical clustering scheme. Similar to DBSCAN, HDBSCAN does not require the number of clusters to be defined beforehand, and it will ignore noisy data points. We use HDBSCAN to cluster H(t,k) and use each cluster's centroid as a source signal mixing vector. We then join these vectors to form the mixing matrix, K, which we use to separate the source signals from ambient magnetic field via compressive sensing.

2.4 Ambient Field Reconstruction

To separate the stray magnetic field signals from the ambient magnetic field, we first estimate the mixing matrix, K, using HDBSCAN. Then, we use compressive sensing (CS) to reconstruct the ambient magnetic field signal from the mixed signals. CS is an algorithm that can recover sparse or near-sparse signals from under-sampled measurements (Baraniuk, 2007). It is widely used in audio and image decompression applications. Hoffmann and Moldwin (2022) apply a weighted Basis Pursuit scheme for CS, which solves the following optimization problem in equation 9 (Candès et al., 2008).

$$\begin{aligned} &\text{Minimize} && w^T|s| \\ &\text{Subject to} && b = Ks \end{aligned} \tag{9}$$

However, this scheme assumes that there is no measurement error in b. If the measured signals are very noisy, this assumption may not hold. Therefore, we propose a different scheme based on the Dantzig Selector with an iterative weighting scheme (Candes & Tao, 2007). The Dantzig Selector relaxes the equality constraint in equation 9 by allowing some error tolerance (Rani et al., 2018). The formulation of the Dantzig Selector is shown in equation 10.

$$\begin{aligned} &\text{Minimize} && w^T|s| \\ &\text{Subject to} && \|K^T(b - Ks)\|_\infty \leq \eta \end{aligned} \tag{10}$$

The parameter, η, in the problem constraint is a tuning parameter that controls how much error is allowed. This formulation enables us to recover the ambient magnetic field signal even when there is some measurement error, e, in the underdetermined measurement system $b = Ks + e$.

We use a weighting scheme to reduce noise and error in the signal reconstruction process. The weighting scheme assigns different importance to different elements in the solution vector, s, which represents the separated signals. The first element of s, denoted by s_0, corresponds to the ambient magnetic field signal, which is our main interest. The other elements correspond to the stray magnetic field signals, which are considered as noise. Hoffmann and Moldwin (2022) use a constant weighting matrix that gives more weight to s_0 than to other elements of s. However, this may not be optimal for different types of mixed signals. Therefore, we propose an adaptive weighting scheme that adjusts the weight of s_0 based on whether the mixed time-frequency signal, B(t,k), is a SSP or a MSP. A SSP means that only one source signal contributes to B(t,k), while an MSP means that multiple source signals contribute to B(t,k). If B(t,k) is a SSP, we use the Candès et al. (2008) weighting scheme where $w = \dfrac{1}{|s|}$, which assigns less weight to larger elements of s to induce sparsity. If B(t,k) is an MSP, we iteratively increase the weight of s_0 using the formula $w[0] = w[0] + \alpha(s_{ratio} - w[0])$, where α is a learning rate and s_{ratio} is the ratio of the sum of absolute values of noise signals to the absolute value of ambient magnetic field signal. The variable, s_{ratio}, is defined in the following equation where s is the solution vector and ϵ is a small constant to prevent division by zero.

$$s_{ratio} = \frac{\sum_{i=1}^{n} |s_i|}{|s_0| + \epsilon} \tag{11}$$

This scheme aims to enhance the sparsity of s by suppressing noise signals and highlighting ambient magnetic field signal. We use this adaptive weighting scheme with Dantzig Selector, which is a compressive sensing recovery method that can handle measurement errors. This system allows us to reconstruct the ambient magnetic field with as little noise as possible from under-sampled measurements.

We use CVXPY, a Python-embedded modeling language for convex optimization problems (Diamond & Boyd, 2016), to solve the system defined by equation 10. CVXPY automatically transforms the problem into standard form, calls a solver, and unpacks the results. The solver we use is Embedded Conic Solver (ECOS), which converts the problem into a Second Order Cone Problem (SOCP) and applies an interior point solver to find the sparse solution (Alizadeh & Goldfarb, 2003; Domahidi et al., 2013).

The final step of our method is to apply a Savitzky-Golay (SG) filter to the reconstructed ambient magnetic field signal. The SG filter is a smoothing technique that preserves the shape and features of the signal while reducing random normal noise. It works by fitting a polynomial of a given order to a sliding window of data points using least squares. The filtered value at each point is obtained by evaluating the fitted polynomial at the center of the window. Liu et al. (2016) used a SG filter to denoise seismological measurements. In our case, we use a SG filter to enhance the quality of the ambient magnetic field signal after compressive sensing recovery.

3 Experimental Data and Results

In this paper, we present two experiments that show the effectiveness of our integrated Quad-Mag and UBSS system for removing stray magnetic fields. The first experiment uses a Mock CubeSat designed by Deshmukh et al. (2020) with four copper coils driven by waveform generators to create artificial noise signals. We also add geomagnetic perturbation data from the SWARM satellite to simulate the ambient magnetic field. The second experiment is a simulation that applies our system to different sizes of CubeSats (1U, 2U, 3U, and 6U). We use the same SWARM data and four noise signals for each simulation. The results demonstrate that our system can successfully remove the stray magnetic fields from these CubeSat configurations.

Figure 5 illustrates the signal processing procedures detailed in sections 2.2-2.4. The first step (i) is to transform the mixed magnetometer signals, b(t), into the time-frequency domain, B(t,k), using the NSGT to improve signal sparsity. The second step (ii) is to remove the low magnitude time-frequency points using the magnitude filter described in equation 5. The third step (iii) is to identify the remaining data points as SSPs or MSPs based on equation 6. The fourth step (iv) is to prepare the data for cluster analysis by transforming it into a clusterable form through equations 4, 7, and 8. The clusterable data, H(t,k), is then used to find the mixing matrix, K, in the fifth step (v) through the use of HDBSCAN. The sixth step (vi) is to separate the original time-frequency data, B(t,k), through the iteratively weighted compressive sensing scheme detailed in section 2.4. Lastly, the SG filter is applyed in the seventh step (vii) in order to reduce the random normal noise of the reconstructed signal.

We use three metrics to evaluate how well our algorithm reconstructs the ambient magnetic field signal from the noisy measurements: Signal to Noise Ratio (SNR), Pearson Correlation Coefficient (ρ), and Root Mean Squared Error (RMSE). These metrics compare the reconstructed signal, x, with the true signal, y, element-wise over the entire time-series. The Pearson Correlation Coefficient, given by equation 12, measures how linearly related the normalized input and recovered signals are.

$$\rho = \frac{\sum_{i=0}^{N-1}(x_i - \bar{x})(y_i - \bar{y})}{\sqrt{\sum_{i=0}^{N-1}|(x_i - \bar{x})|^2 \sum_{i=0}^{N-1}|(y_i - \bar{y})|^2}} \tag{12}$$

The RMSE, given by equation 13, measures the average magnitude of error between the estimated and true signals. This metric is sensitive to large outliers, so a few large deviations may inflate its value. The RMSE does not indicate what an acceptable level of error is, so we also use the SNR.

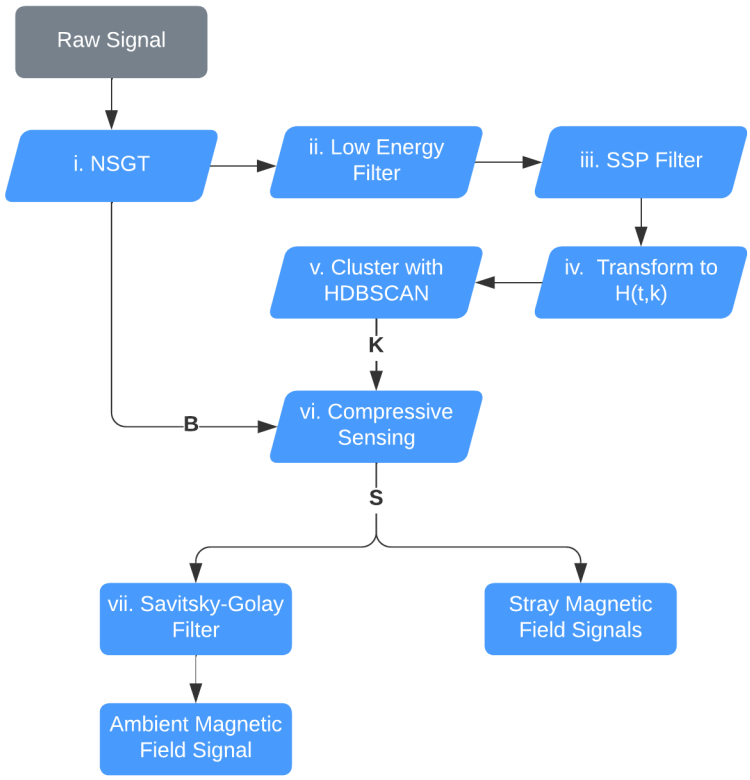

Figure 5: Block diagram of the processes involved in recovering the mixing matrix, $\mathbf{K}$, through cluster analysis and reconstructing the ambient magnetic field signal, S_0, through compressed sensing.

$$RMSE = \sqrt{\frac{\sum_{i=0}^{N-1}(x_i - y_i)^2}{N}} \tag{13}$$

The SNR, measured in decibels, defines the ratio of power from the ambient magnetic field signal to power from noise from stray magnetic field signals. This metric helps to give context to the RMSE value. The SNR is given by equation 14.

$$SNR = 10\log_{10}\frac{\sum_{i=1}^{n}(x_i - \bar{x})^2}{\sum_{i=1}^{n}(x_i - y_i)^2} \tag{14}$$

3.1 Experiment 1: Mock CubeSat Noise Removal

In this experiment, we demonstrate the utility of the proposed algorithm on real magnetic field data. To take measurements of the copper coil-generated noise signals, we used a prototype of the Quad-Mag magnetometer. The copper coils were driven by signal generators to create the source signals, $s(t) \supset [s_2(t), s_3(t), s_4(t), s_5(t)]$. The waveforms driving the stray magnetic field signals were a 5 Hz sine wave, 2 Hz sawtooth wave, 0.8 Hz sine wave, and a 3 Hz attenuating sine wave. The spectral content of these noise signals provided a variety of sparse and wideband signals to test against. The Quad-Mag sampled 150 seconds of the coil-generated signals at 65 Hz. A single PNI RM3100 magnetometer has an estimated measurement uncertainty of 10.5 nT at 65 Hz. The aver-

aged Quad-Mag measurements are estimated to have a factor of 2 reduction in measurement uncertainty, near 5.25 nT. The experimental apparatus is shown in Figure 6.

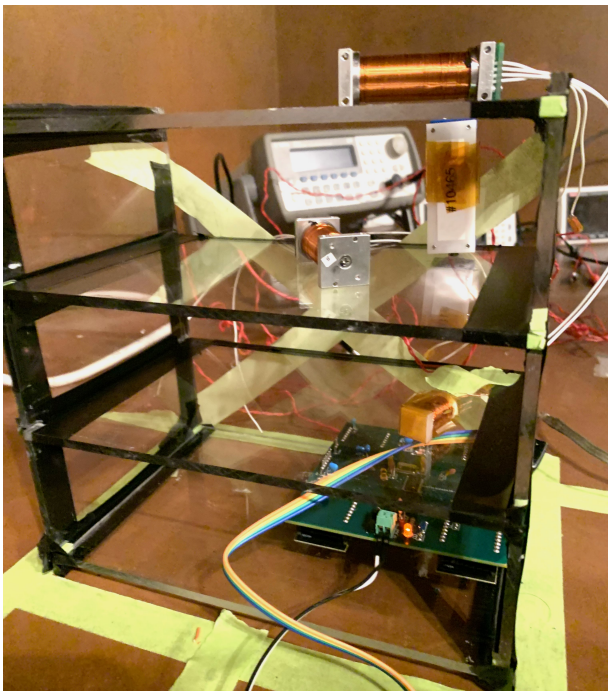

Figure 6: The Quad-Mag and copper coils are placed within the mock CubeSat to emulate a 3U CubeSat. The Quad-Mag is located at the bottom of the CubeSat, while the four noise coils are placed vertically above it, all contained within a 10x10cm^2 area. The mock CubeSat is housed in a copper room lined with mu-metal to provide magnetic shielding. This room serves as a large magnetic shield.

The source signals were combined in the mixing system, $b(t) = Ks(t) = [b_1(t), b_2(t), b_3(t), b_4(t)]$. The signal, $s_1(t)$, was residual geomagnetic field data that was generated by subtracting the IGRF model from spacecraft magnetic field data measured by the SWARM A satellite. The data were recorded on March 17th, 2015, between 8:53 and 8:55 UTC as the spacecraft passed through a perturbation in the southern auroral zone. The first twenty seconds of the mixed signals are shown in Figure 7.

The UBSS algorithm was applied to the Quad-Mag's z-axis following the procedure in Figure 5. In step one (i), the NSGT algorithm requires the user to set the lowest frequency for the transform and the bands per octave. We set the low frequency to 0.01 Hz and used 1 band per octave. These values are used to vary the window length with respect to the frequency being analyzed. In the second step (ii), we used $\sigma = 10$ and $\lambda = 2$ to remove low-energy points. The value σ corresponds to the estimated noise at a single magnetometer of about 10.5 nT. In the third step (iii), the time-frequency points were classified as MSPs and removed if they had an angle above $\theta = 15°$. The next two steps of the algorithm require no user-set parameters. The noise signals were identified using cluster analysis and separated using compressive sensing. After separation, the ambient magnetic field signal is smoothed with a SG filter that uses a sliding window of 33 data points and a third order polynomial. The cleaned magnetic field signal and the spectra of the noisy, cleaned, and true signal are shown in Figure 8.

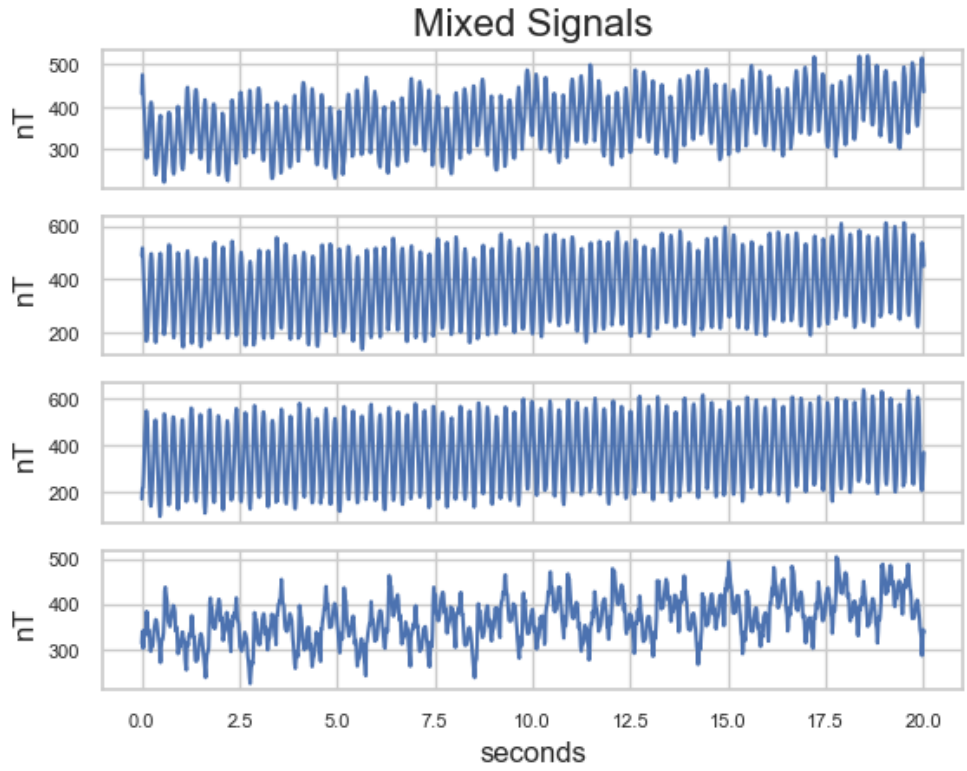

Figure 7: Plots (a), (b), (c), and (d) show 20 seconds of the four mixed signals recorded by the Quad-Mag at 65 Hz. The four noise signals are a 5 Hz sine wave, 2 Hz sawtooth wave, 0.8 Hz sine wave, and a 3 Hz attenuating sine wave. The fifth source signal is the ambient magnetic field signal added virtually to each magnetometer signal. The noise signals have amplitudes between 50 nT and 200 nT.

The estimated ambient magnetic field signal in Figure 8 closely resembles the true geomagnetic field signal. Table 1 shows the RMSE, SNR, and correlation of the reconstructed signal with respect to the true magnetic field signal. We compared these results to a single magnetometer on the Quad-Mag and to the average of all four magnetometers to demonstrate the efficacy of our algorithm and the integrated suite. The results of the algorithm without the SG filter applied are included in the supplement of this paper.

Table 1: Summary of Experiment 1 Results.

	ρ	**SNR (dB)**	**RMSE (nT)**
Single	0.4353	-6.29	120.07
Average	0.9518	9.84	18.72
UBSS	0.9971	22.33	4.40

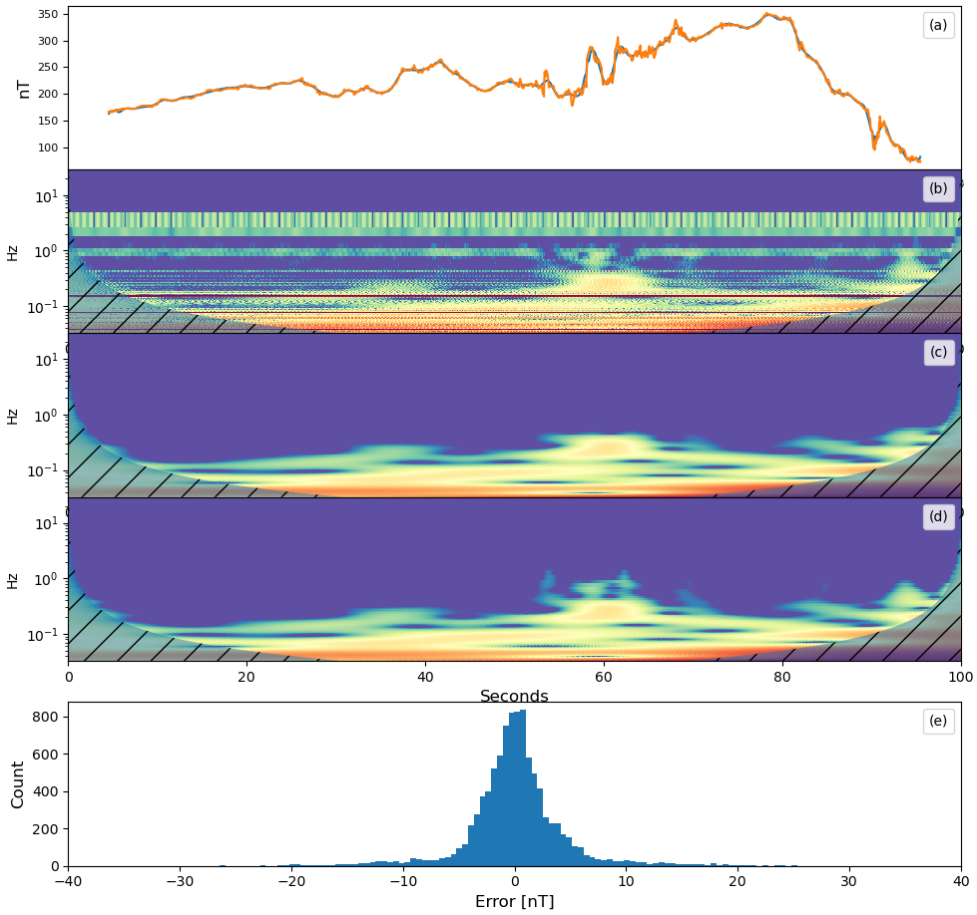

Figure 8: The blue line in plot (a) represents the magnetometer signal after cleaning, while the orange line shows the actual ambient magnetic field signal. Plot (b) displays a scaleogram of the raw signal from a single magnetometer on the Quad-Mag, created using wavelet analysis. The shaded regions indicate invalid wavelet results. Plot (c) shows a scaleogram of the estimated ambient magnetic field signal, and plot (d) shows a scaleogram of the true signal. Plot (e) is a histogram of the error between the original and estimated signals, $s_1 - \hat{s}_1$.

3.2 Experiment 2: Simulated CubeSat Noise Removal

In this simulation, we investigate the performance of the UBSS algorithm in removing noise signals from magnetometer measurements for several CubeSat form factors. We use the magpylib package to simulate a four dipole noise sources and four virtual magnetometers. The magnetometers are placed to emulate the spacing and function of the Quad-Mag. The noise sources consist of simulated reaction wheel noise signal, square wave and sine wave signals that turn on and off randomly, and real magnetometer noise from the Michibiki satellite. The Michibiki magnetometer data used is a full 24-hour measurement from April 23rd, 2012 (Imajo et al., 2021). The noise signal was created by subtracting the inboard and outboard magnetometers to remove the geomagnetic field and resampling the signal to fit the 100 second window of the simulated signals. This introduces a frequency shift in the Michibiki noise signal but maintains the same spectral structures. The source signals used in this experiment are shown in Figure 9.

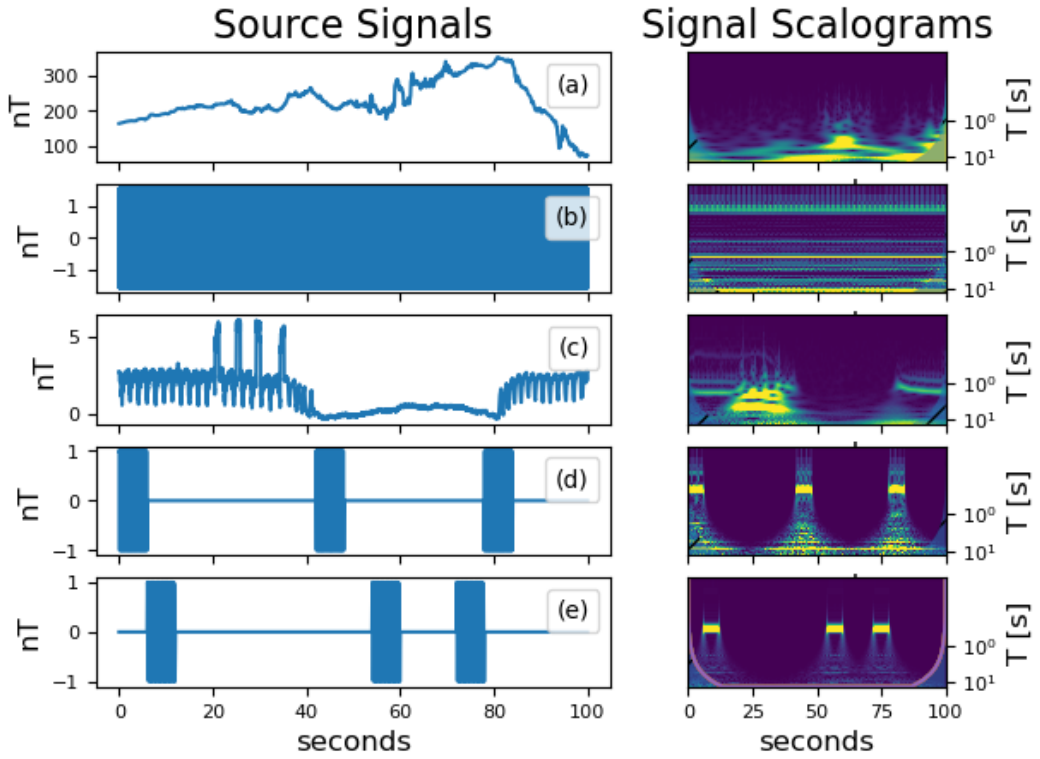

Figure 9: Five source signals sampled at 50 Hz. Panel (a) shows the SWARM geomagnetic field data used as the ambient signal. Panel (b) shows a simulated reaction-wheel signal that has 15 Hz and 20 Hz components. Panel (c) shows real spacecraft noise taken measured by Michibiki-1. Panel (d) and panel (c) show a 5 Hz square wave and 3 Hz sine wave turning on and off randomly. The second column shows the wavelet scalogram of each source signal. The y-axis is the period of the signal in seconds. The coloring shows the normalized amplitude of the detrended signals.

The Magpylib python library was used to simulate these source signals as magnetic fields. Magpylib allows the user to specify the location of various magnetic field sources and magnetometers. The library is not able to simulate AC magnetic fields, however, we overcome this by measuring each noise source at each magnetometer and forming a mixing matrix, K. The magnetometer signals are then generated by multiplying the source signals, s, by the mixing matrix, K, in the system, $b(t) = Ks(t)$. This method does not take into account any induction currents or the presence of conductors that may be present in spacecraft. Additionally, we used dipole fields to simulate the magnetic fields of the noise sources. The first twenty seconds of mixed virtual magnetometer signals are shown in Figure 10.

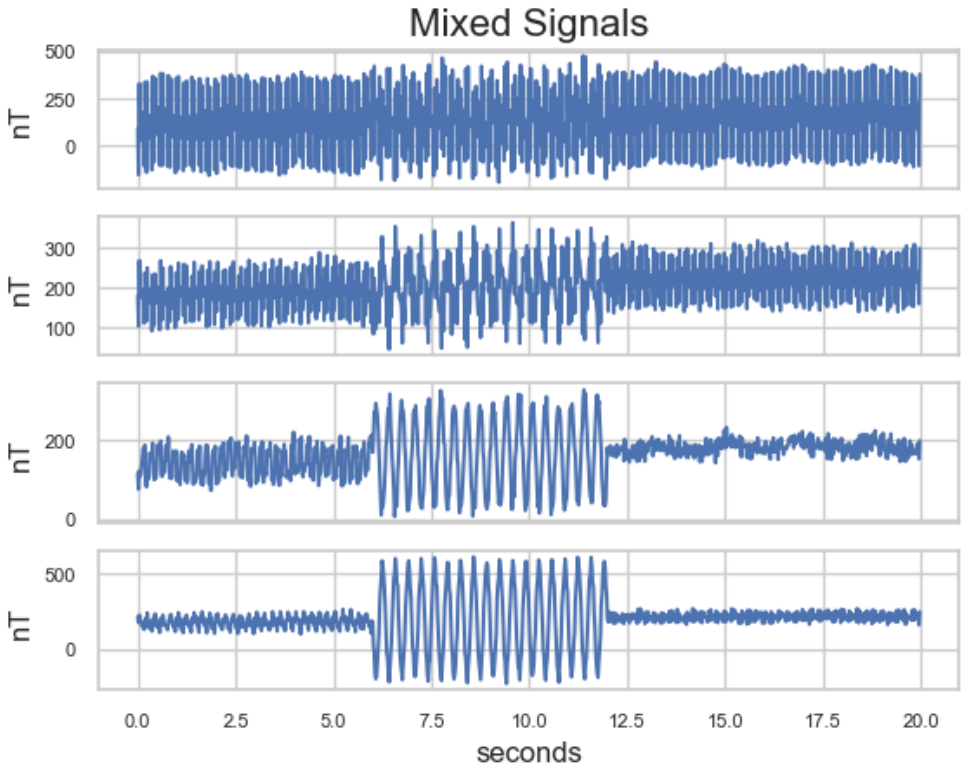

Figure 10: Plots (a), (b), (c), and (d) show 20 seconds of the four mixed signals recorded by the Quad-Mag at 50 Hz in the 1U spacecraft configuration. The four mixed signals respresent a combination of the real and simulated noise signals shown in Figure 9. The SWARM geomagnetic perturbation data was added to each magnetometer equally as well as 10 nT of random normal noise. The noise signals have amplitudes up to near 400 nT peak to peak at a single magnetometer.

The noise sources were placed randomly within a 1U volume and were scaled vertically and horizontally to simulate the 2U, 3U, and 6U CubeSats. The locations of the noise sources and virtual magnetometers in the 1U CubeSat magpylib simulation are shown in Figure 11.

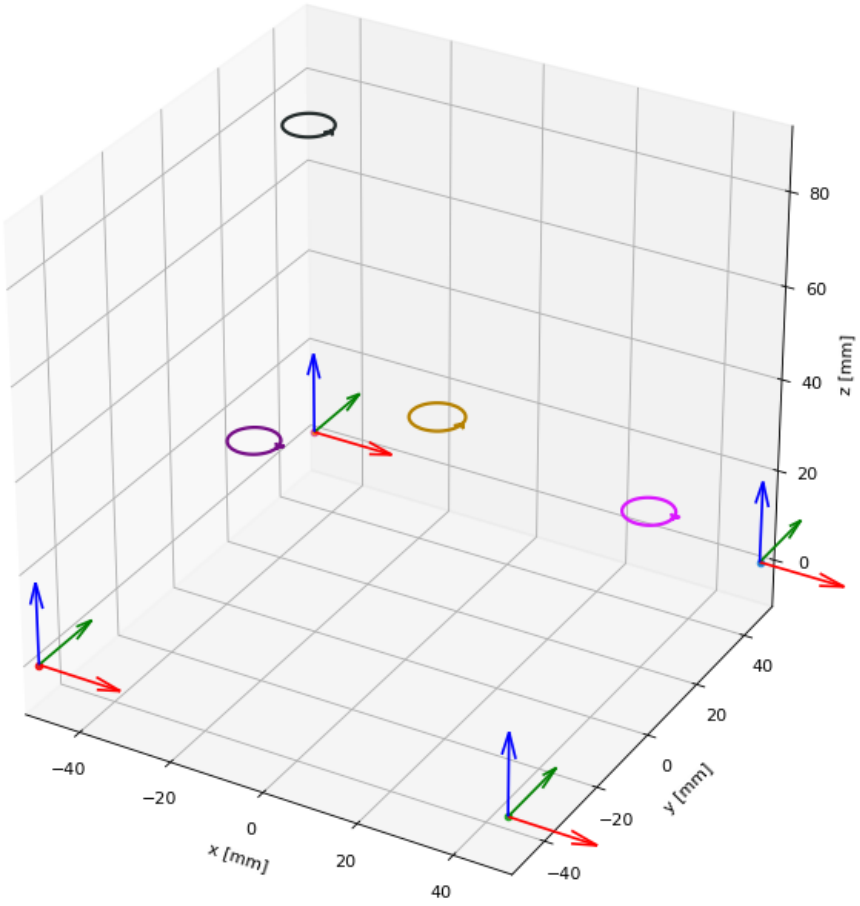

Figure 11: Noise source locations and virtual magnetometers in a 1U CubeSat simulation. The circles represent dipole noise sources with locations (x,y,z) in millimeters: (43, 16, 27), (-36, 26, 83), (25, -32, 66), and (-25, -13, 37). The tri-color vectors represent virtual magnetometers. The noise source locations were scaled proportionally for simulations of 2U, 3U, and 6U CubeSats.

The magnetometer measurements were sampled at a rate of 50 Hz and 10 nT of random normal noise was added to each magnetometer signal. The UBSS algorithm was applied to the virtual x-axis for each CubeSat following the procedure in Figure 5. In step one (i), the NSGT algorithm requires the user to set the lowest frequency for the transform and the bands per octave. We set the low frequency to 0.1 Hz and used 1 band per octave. In the second step (ii), we used $\sigma = 10$ and $\lambda = 5$ to remove low-energy points. The value σ corresponds to the estimated noise at a single magnetometer of 10 nT. In the third step (iii), MSPs were removed if they had an angle above $\theta = 10°$. Finally, the noise signals were identified using cluster analysis and separated using compressive sensing. Table 2 shows the results of the UBSS algorithm with respect to simply taking an average of all of the magnetometers signals.

Table 2: Summary of Experiment 2 Results.

	Metric	**1U**	**2U**	**3U**	**6U**
RMSE	Single	163.24	158.62	52.04	273.09
	Average	62.71	140.25	85.3	140.71
	UBSS	3.83	5.33	8.08	4.16
ρ	Single	0.4095	0.411	0.7601	0.2167
	Average	0.7054	0.4062	0.5643	0.3892
	UBSS	0.9978	0.9961	0.9926	0.9977
SNR	Single	-9.15	-8.90	0.78	-13.62
	Average	-0.84	-7.83	-3.51	-7.86
	UBSS	23.44	20.58	16.95	22.72

4 Discussion and Future Work

We present an integrated magnetometer suite that combines the Quad-Mag CubeSat magnetometer for distributed magnetic field measurements and UBSS for noise removal. The use of four embedded magnetometers in the Quad-Mag lowers the instrument noise by a factor of two and enables noise removal algorithms. To validate this system, we performed two experiments. The first experiment used a prototype Quad-Mag and stray magnetic fields generated by current-driven copper coils. A single magnetometer on the Quad-Mag board had an RMSE of 120.07 nT and a SNR of -6.29 dB. The averaged Quad-Mag signal improved these metrics to 18.72 nT and 9.84 dB, respectively. After applying UBSS to the Quad-Mag signals, we reconstructed the magnetic field signal with an RMSE of 4.4 nT and a SNR of 22.33 dB. This is below both the measurement error expected at 65 Hz for a single magnetometer (near 10.5 nT) and also below the theoretical noise level for the averaged Quad-Mag error (i.e., factor of 2 reduction due to four sensors). This surprising result may be due to the unique weighting algorithm used in the compressive sensing stage, which zeros out the random normal noise of low-SNR time-frequency bins but keeps it in high-SNR bins. The residual error between the true and estimated signals In Figure 8 Panel (e) showed a normal distribution, indicating that UBSS successfully identified and removed every noise signal.

We performed a second experiment to test the efficacy of UBSS when applied to different CubeSat sizes. We simulated four different CubeSat form factors (1U, 2U, 3U, and 6U) with noise sources scaled accordingly. The placement of the virtual magnetometers mimicked the Quad-Mag design, and 10 nT of random normal noise was added to simulate the measurement uncertainty at 50 Hz. In addition, real magnetometer noise from the Michibiki satellite is used as a source signal in these simulations. As a result, any random normal noise from the Michibiki satellite magnetometers also adds to the simulated 10 nT of normal noise. For the 1U CubeSat, UBSS reduced the error from 163.24 nT at a single magnetometer to 3.83 nT. This is below both the expected normal error of 10 nT for a single magnetometer and the normal error 5 nT for the averaged magnetometer. However, the RMSE of the reconstructed signal did not strictly decrease as we scaled the noise sources vertically away. The average signal error for the 2U, 3U, and 6U CubeSats were 140.25 nT, 85.3 nT, and 140.71 nT, respectively. UBSS outperformed these averages with an RMSE of 5.33 nT, 8.08 nT, and 4.16 nT, respectively. This experiment demonstrates that UBSS can successfully remove CubeSat noise for various CubeSat form factors, but it also suggests that the position of the noise sources relative to the magnetometers affects the efficacy of the algorithm. The Restricted Isometry Property (RIP) is a condition that ensures that compressive sensing can reconstruct the source signals in the presence of noise (Candès, 2008). The mixing matrix in UBSS is the matrix that connects the noise sources to the magnetometer measurements, and it should satisfy the RIP for successful noise separation. Altering the location of the noise sources will change the RIP and may affect signal reconstruction.

One of the key assumptions of UBSS is that the ambient magnetic field is uniform across all magnetometers. A potential flaw to this assumption is that a stray magnetic field signal that appears equally at each magnetometer may be construed with the ambient magnetic field. As a result, the UBSS algorithm may not be able to separate the stray magnetic field signal from the ambient magnetic field. To avoid this issue, we suggest placing the magnetometers or the spacecraft subsystems in such a way that minimizes this possibility. Furthermore, UBSS relies on the sparsity of the noise sources in a certain transform domain to apply compressive sensing techniques for signal separation. In this work, we use NSGT to achieve higher sparsity of the noise signals. However, the sparsity assumption may not be valid for all kinds of noise sources or transform domains.

In summary, we present a novel method to remove noise signals from magnetometer measurements using the Quad-Mag CubeSat magnetometer and the UBSS algorithm. Compared to a single magnetometer or the averaged Quad-Mag signals, our method achieves better RMSE, SNR, and correlation with the true magnetic field signal. However, our simulations and experiments are based on a simplified stray magnetic field model and may not capture the complexity of real spacecraft magnetic fields. To address this limitation, future work includes characterizing spacecraft magnetic fields and using the characterized field equations in magpylib simulations, and integrating the Quad-Mag into a real CubeSat and testing its performance. Additionally, we introduced a novel iterative weighting algorithm that relies on SSP detection. This algorithm presents a significant improvement to preferentially reconstructing the ambient magnetic field signal, but further work is necessary to validate and improve the MSP weighting scheme.

5 Conclusions

This work presents a new approach for obtaining high-fidelity magnetic field measurements from CubeSats using the Quad-Mag magnetometer and UBSS. The Quad-Mag instrument, equipped with four magneto-inductive magnetometers, provides a resolution that is two times greater than that of any single sensor. The UBSS algorithm effectively removes stray magnetic field noise without prior knowledge of the magnitude, orienta-

tion, or number of noise sources. The combination of the Quad-Mag and UBSS allows for boomless magnetic field measurements with a high degree of accuracy and precision.

We performed two experiments to validate the integrated Quad-Mag and UBSS suite. The first experiment demonstrated the removal of four noise signals generated by copper coils from geomagnetic field data added virtually to the Quad-Mag measurements. This experiment showed a reduction of stray magnetic field noise from 120.07 nT at a single magnetometer to 4.40 nT when sampled at 65 Hz. This is below the expected measurement error of 10.5 nT for a single PNI RM3100 sampled at that rate. The second experiment simulated the removal of four noise signals in several CubeSat configurations. The stray magnetic field signals were composed of real spacecraft noise taken from the Michibiki satellite and artificial noise signals turning on and off randomly. The UBSS algorithm reduced the error of the measured magnetometer signals from 163.24 nT to 3.83 nT in the 1U CubeSat simulation.

The results of this study demonstrate the potential of the Quad-Mag and UBSS package as a reliable and cost-effective solution for in situ magnetic field measurements in CubeSats. The Quad-Mag and UBSS package has the potential to revolutionize the way magnetic field measurements are conducted from CubeSats, making it a valuable tool for space research, exploration, and attitude control. The ability to conduct high-fidelity magnetic field measurements without the need for a boom can open new possibilities for CubeSat missions, enabling scientists without access to expensive spacecraft platforms to propose and study a wide range of space phenomena.

Data Availability Statement

The SWARM magnetometer data are available from `https://swarm-diss.eo.esa.int` under MAGx_HR in the Level 1B data products folder. The Michibiki QSZ-1 Magnetometer data is available at `https://sees.tksc.jaxa.jp/fw/dfw/SEES/English/Papers/data/2020/peer_reviewed/01/2020_reviewed_01.shtml`. The noise signals generated in simulation and in the laboratory are available on the University of Michigan Deep Blue data repository (`Todo`).

Acknowledgments

Work at the University of Michigan was supported by NASA grants 80NSSC19K0608 and 80NSSC18K1240. The SWARM perturbation data were provided by Dr. Yining Shi. The mock CubeSat used in this work was created by Dr. Srinagesh Sharma.

References

Alizadeh, F., & Goldfarb, D. (2003, January). Second-order cone programming. *Mathematical Programming*, *95*(1), 3–51. Retrieved 2022-05-12, from `http://link.springer.com/10.1007/s10107-002-0339-5` doi: 10.1007/s10107-002-0339-5

Baraniuk, R. G. (2007, July). Compressive Sensing [Lecture Notes]. *IEEE Signal Processing Magazine*, *24*(4), 118–121. (Conference Name: IEEE Signal Processing Magazine) doi: 10.1109/MSP.2007.4286571

Califf, S., Early, D., Grotenhuis, M., Loto'aniu, T. M., & Kronenwetter, J. (2020). Correcting the Arcjet Thruster Disturbance in GOES-16 Magnetometer Data. *Space Weather*, *18*(1), e2019SW002347. Retrieved 2023-02-20, from `https://onlinelibrary.wiley.com/doi/abs/10.1029/2019SW002347` (_eprint: https://onlinelibrary.wiley.com/doi/pdf/10.1029/2019SW002347) doi: 10.1029/2019SW002347

Campello, R. J. G. B., Moulavi, D., & Sander, J. (2013). Density-Based Clustering Based on Hierarchical Density Estimates. In J. Pei, V. S. Tseng,

L. Cao, H. Motoda, & G. Xu (Eds.), *Advances in Knowledge Discovery and Data Mining* (pp. 160–172). Berlin, Heidelberg: Springer. doi: 10.1007/978-3-642-37456-2_14

Candes, E., & Tao, T. (2007, December). The Dantzig selector: Statistical estimation when p is much larger than n. *The Annals of Statistics*, *35*(6). Retrieved 2023-03-01, from http://arxiv.org/abs/math/0506081 (arXiv:math/0506081) doi: 10.1214/009053606000001523

Candès, E. J. (2008). The restricted isometry property and its implications for compressed sensing. *C. R. Acad. Sci. Paris, Ser. I*, *346*, 589–592. doi: 10.1016/j.crma.2008.03.014

Candès, E. J., Wakin, M. B., & Boyd, S. P. (2008, December). Enhancing Sparsity by Reweighted 1 Minimization. *Journal of Fourier Analysis and Applications*, *14*(5), 877–905. Retrieved 2023-03-01, from https://doi.org/10.1007/s00041-008-9045-x doi: 10.1007/s00041-008-9045-x

Carter, D., Freesland, D., Tadikonda, S. K., Kronenwetter, J., Todirita, M., Dahya, M., & Chu, D. (2016, May). Correcting GOES-R magnetometer data for stray fields. In *2016 ESA Workshop on Aerospace EMC (Aerospace EMC)* (pp. 1–6). Valencia, Spain: IEEE. Retrieved 2023-02-20, from http://ieeexplore.ieee.org/document/7504597/ doi: 10.1109/AeroEMC.2016.7504597

Deshmukh, A. A., Sharma, S., Cutler, J. W., Moldwin, M., & Scott, C. (2020, February). Simple Regret Minimization for Contextual Bandits. *arXiv:1810.07371 [cs, stat]*. Retrieved 2021-07-23, from http://arxiv.org/abs/1810.07371 (arXiv: 1810.07371)

Diamond, S., & Boyd, S. (2016). CVXPY: A Python-embedded modeling language for convex optimization. *Journal of Machine Learning Research*, *17*(83), 1–5.

Domahidi, A., Chu, E., & Boyd, S. (2013, July). ECOS: An SOCP solver for embedded systems. In *2013 European Control Conference (ECC)* (pp. 3071–3076). Zurich: IEEE. Retrieved 2021-08-18, from https://ieeexplore.ieee.org/document/6669541/ doi: 10.23919/ECC.2013.6669541

Ester, M., Kriegel, H.-P., & Xu, X. (n.d.). A Density-Based Algorithm for Discovering Clusters in Large Spatial Databases with Noise. , 6.

Finley, M. G., Broadfoot, R. M., Shekhar, S., & Miles, D. M. (2023). Identification and Removal of Reaction Wheel Interference From In-Situ Magnetic Field Data Using Multichannel Singular Spectrum Analysis. *Journal of Geophysical Research: Space Physics*, *128*(2), e2022JA031020. Retrieved 2023-03-09, from https://onlinelibrary.wiley.com/doi/abs/10.1029/2022JA031020 (_eprint: https://onlinelibrary.wiley.com/doi/pdf/10.1029/2022JA031020) doi: 10.1029/2022JA031020

Hoffmann, A. P., & Moldwin, M. B. (2022). Separation of Spacecraft Noise From Geomagnetic Field Observations Through Density-Based Cluster Analysis and Compressive Sensing. *Journal of Geophysical Research: Space Physics*, *127*(9), e2022JA030757. Retrieved 2023-02-19, from https://onlinelibrary.wiley.com/doi/abs/10.1029/2022JA030757 (_eprint: https://onlinelibrary.wiley.com/doi/pdf/10.1029/2022JA030757) doi: 10.1029/2022JA030757

Holighaus, N., Dorfler, M., Velasco, G. A., & Grill, T. (2013, April). A Framework for Invertible, Real-Time Constant-Q Transforms. *IEEE Transactions on Audio, Speech, and Language Processing*, *21*(4), 775–785. Retrieved 2022-05-03, from http://ieeexplore.ieee.org/document/6384709/ doi: 10.1109/TASL.2012.2234114

Imajo, S., Nosé, M., Aida, M., Matsumoto, H., Higashio, N., Tokunaga, T., & Matsuoka, A. (2021, May). Signal and Noise Separation From Satellite Magnetic Field Data Through Independent Component Analysis: Prospect of Magnetic Measurements Without Boom and Noise Source Information. *Journal*

of Geophysical Research: Space Physics, *126*(5). Retrieved 2021-06-30, from https://onlinelibrary.wiley.com/doi/10.1029/2020JA028790 doi: 10.1029/2020JA028790

Kilcommons, L. M., Redmon, R. J., & Knipp, D. J. (2017). A new DMSP magnetometer and auroral boundary data set and estimates of field-aligned currents in dynamic auroral boundary coordinates. *Journal of Geophysical Research: Space Physics*, *122*(8), 9068–9079. Retrieved 2021-11-02, from https://onlinelibrary.wiley.com/doi/abs/10.1002/2016JA023342 (_eprint: https://onlinelibrary.wiley.com/doi/pdf/10.1002/2016JA023342) doi: 10.1002/2016JA023342

Leuzinger, A., & Taylor, A. (2010). *Magneto-inductive technology overview.* PNI White Paper.

Liu, Y., Dang, B., Li, Y., Lin, H., & Ma, H. (2016, February). Applications of Savitzky-Golay Filter for Seismic Random Noise Reduction. *Acta Geophysica*, *64*(1), 101–124. Retrieved 2023-03-13, from https://doi.org/10.1515/acgeo-2015-0062 doi: 10.1515/acgeo-2015-0062

McInnes, L., & Healy, J. (2017). Accelerated hierarchical density based clustering. In *2017 ieee international conference on data mining workshops (icdmw)* (p. 33–42).

Miller, D. C. (1979, April). The Voyager magnetometer boom.. Retrieved 2023-02-20, from https://ntrs.nasa.gov/citations/19790013187 (NTRS Author Affiliations: Jet Propulsion Lab., California Inst. of Tech. NTRS Document ID: 19790013187 NTRS Research Center: Legacy CDMS (CDMS))

Moldwin, M. B., Wilcox, E., Zesta, E., & Bonalsky, T. M. (2022, June). Single-event effect testing of the PNI RM3100 magnetometer for space applications. *Geoscientific Instrumentation, Methods and Data Systems*, *11*(1), 219–222. Retrieved 2023-02-19, from https://gi.copernicus.org/articles/11/219/2022/ (Publisher: Copernicus GmbH) doi: 10.5194/gi-11-219-2022

Ness, N. F., Behannon, K. W., Lepping, R. P., & Schatten, K. H. (1971). Use of two magnetometers for magnetic field measurements on a spacecraft. *Journal of Geophysical Research (1896-1977)*, *76*(16), 3564–3573. Retrieved 2021-07-23, from https://agupubs.onlinelibrary.wiley.com/doi/abs/10.1029/JA076i016p03564 (_eprint: https://agupubs.onlinelibrary.wiley.com/doi/pdf/10.1029/JA076i016p03564) doi: 10.1029/JA076i016p03564

Rani, M., Dhok, S. B., & Deshmukh, R. B. (2018). A Systematic Review of Compressive Sensing: Concepts, Implementations and Applications. *IEEE Access*, *6*, 4875–4894. (Conference Name: IEEE Access) doi: 10.1109/ACCESS.2018.2793851

Ream, J. B., Weiss, B. P., Oran, R., Raymond, C. A., Polanskey, C. A., Wenkert, D. D., ... Merayo, J. M. G. (2021, November). Magnetic gradiometry using frequency-domain filtering. *Measurement Science and Technology*, *33*(1), 015104. Retrieved 2022-01-14, from https://doi.org/10.1088/1361-6501/ac2e2e (Publisher: IOP Publishing) doi: 10.1088/1361-6501/ac2e2e

Regoli, L. H., Moldwin, M. B., Pellioni, M., Bronner, B., Hite, K., Sheinker, A., & Ponder, B. M. (2018, March). Investigation of a low-cost magneto-inductive magnetometer for space science applications. *Geoscientific Instrumentation, Methods and Data Systems*, *7*(1), 129–142. Retrieved 2023-02-17, from https://gi.copernicus.org/articles/7/129/2018/ (Publisher: Copernicus GmbH) doi: 10.5194/gi-7-129-2018

Regoli, L. H., Moldwin, M. B., Raines, C., Nordheim, T. A., Miller, C. A., Carts, M., & Pozzi, S. A. (2020, December). Radiation tolerance of the PNI RM3100 magnetometer for a Europa lander mission. *Geoscientific Instrumentation, Methods and Data Systems*, *9*(2), 499–507. Retrieved 2023-02-21, from https://gi.copernicus.org/articles/9/499/2020/ (Publisher: Coper-

nicus GmbH) doi: 10.5194/gi-9-499-2020

Reju, V. G., Koh, S. N., & Soon, I. Y. (2009, September). An algorithm for mixing matrix estimation in instantaneous blind source separation. *Signal Processing*, *89*(9), 1762–1773. Retrieved 2023-02-27, from https://www.sciencedirect.com/science/article/pii/S0165168409001157 doi: 10.1016/j.sigpro.2009.03.017

Strabel, B. P., Regoli, L. H., Moldwin, M. B., Ojeda, L. V., Shi, Y., Thoma, J. D., ... Pellioni, M. (2022, November). Quad-Mag board for CubeSat applications. *Geoscientific Instrumentation, Methods and Data Systems*, *11*(2), 375–388. Retrieved 2023-02-19, from https://gi.copernicus.org/articles/11/375/2022/ (Publisher: Copernicus GmbH) doi: 10.5194/gi-11-375-2022

Sun, J., Li, Y., Wen, J., & Yan, S. (2016, January). Novel mixing matrix estimation approach in underdetermined blind source separation. *Neurocomputing*, *173*, 623–632. Retrieved 2021-08-17, from https://www.sciencedirect.com/science/article/pii/S092523121501142X doi: 10.1016/j.neucom.2015.08.008

Wallis, D. D., Miles, D. M., Narod, B. B., Bennest, J. R., Murphy, K. R., Mann, I. R., & Yau, A. W. (2015, June). The CASSIOPE/e-POP Magnetic Field Instrument (MGF). *Space Science Reviews*, *189*(1), 27–39. Retrieved 2023-02-20, from https://doi.org/10.1007/s11214-014-0105-z doi: 10.1007/s11214-014-0105-z